RSC Advances

ROYAL SOCIETY OF CHEMISTRY

www.rsc.org/advances

RSC Advances

PAPER

Preparation of zinc hydroxystannate nanocomposite coated by organophosphorus and investigation of its effect on mechanical properties and flame retardancy of poly (vinyl chloride)

Received 00th January 20xx,
Accepted 00th January 20xx

DOI: 10.1039/x0xx00000x

www.rsc.org/

Ting-Ting Gao, Zhi-Wei Li*, Lai-Gui Yu and Zhi-Jun Zhang

To improve the flame retardancy of flame retardants with the assistance of the synergistic effect between organic flame retardant (vinyl trimethoxy silane grafted by 9,10-dihydro-9-oxa-10-phosphaphenanthrene-10-oxide, DOPO-VTS) and inorganic flame retardant (zinc hydroxystannate nanoparticle, ZHS), a novel organic-inorganic hybrid flame retardant, ZHS nanoparticle coated by DOPO-VTS (DOPO-VTS-ZHS), was successfully prepared and well characterized. Subsequently, DOPO-VTS, ZHS and as-prepared DOPO-VTS-ZHS were separately incorporated into poly(vinyl chloride) (PVC) to form PVC-matrix nanocomposites, and the thermal stability, mechanical properties and flame retardancy of the as-prepared PVC-matrix nanocomposites were investigated. Thermogravimetric analysis results showed that the presence of ZHS, DOPO-VTS or DOPO-VTS-ZHS in the PVC matrix led to a slight thermal destabilization effect under air, which promoted the formation of char residue and increased the char yield at 600 ℃. Limited oxygen index (LOI) tests revealed that they also imparted PVC nanocomposites higher values of LOI over pure PVC. Besides, the cone calorimeter result revealed that the three kind of flame retardants could obviously reduce the peak heat release rate (pHRR) , the total heat release (THR) and smoke products of PVC. Among them, DOPO-VTS-ZHS had the most significant effect. Particularly, with the incorporation of 5 wt.% of DOPO-VTS-ZHS, the pHRR of DOPO-VTS-ZHS/PVC was significantly reduced by 39%, and the THR was decreased by 50%, compared with those of neat PVC. The dramatically reduced fire hazards are generally attributed to the synergistic effect of DOPO-VTS and ZHS, containing good dispersion of DOPO-VTS-ZHS, catalytic char function of DOPO and ZHS. In addition, DOPO-VTS-ZHS nanoparticles are also able to significantly increase the tensile strength of PVC matrix.

1.Introduction

Poly(vinyl chloride) (PVC), a kind of common thermoplastics, is widely used in building materials, sealing strip, wire, and cable [1]; and in particular, flexible PVC containing large amounts of low molecular weight liquid plasticizers that can tailor its physical properties is preferred for such applications [2]. However, the incorporation of organic plasticizer usually makes PVC products easier to burn [3], which means it is imperative to incorporate flame retardants into flexible PVC so as to improve its flame retardancy [4]. Previous studies show that halogenated compounds are capable of improving the flame retardancy of polymers [5]. However, due to the potential health and environmental hazards of halogenated flame retardants, the use of the halogenated flame retardants is limited [6]. Recently, halogen-free flame-retardant polymer materials have received a great deal of attention, due to their desired environmental acceptance [7]. For example, inorganic tin-containing compounds, such as zinc stannate ($ZnSnO_3$) and zinc hydroxystannate [$ZnSn(OH)_6$, ZHS], are well-documented as nontoxic flame-retardant and smoke suppressant additives for a wide range of plastics, rubbers, paints, and other polymeric materials [8-11]. Particularly, ZHS as a highly efficient flame retardant has attracted considerable attention, due to its environment-friendliness and safety [12]. In the meantime, ZHS flame retardant is of special significance, because Zn^{2+} ion can act as a Lewis acid to catalyze esterification and dehydrogenation [13], thereby forming a compact residue layer to provide increased flame retardancy of halogen-free systems [14]. Unfortunately, the nonreactive flame retardant like

Engineering Research Center for Nanomaterials, Henan University, Kaifeng 475004, P.R. China. E-mail: zhiweili@henu.edu.cn; Tel: +86-371-23881358

ZHS is less competitive in some sense, since it might deteriorate material properties (a high content of ZHS may dramatically reduce the cross-link density of polymer; and the elutriation of ZHS may reduce the flame retardancy) [15]. Therefore, it is imperative to incorporate ZHS with good fire safety into polymer matrices with good mechanical properties so as to develop novel high-performance flame retardants.

Viewing the abovementioned, we draw our attention to organic-inorganic hybrid nanocomposites, since they usually possess improved thermal stability and mechanical properties than the inorganic and/or organic bulks, while the organic groups in the organic-inorganic hybrids are conducive to the dispersion of the inorganic substances in the polymer matrix [16-18]. With vinyltrimethoxysilane (VTS) grafted by 9,10-dihydro-9-oxa-10-phosphaphenanthrene-10-oxide (DOPO) as an example, it contains high content of DOPO and silicon. On the one hand, DOPO exhibits excellent flame retardancy, due to its high gas-phase and condensed-phase activity (through char formation) as well as high thermal stability, good oxidation resistance and good water resistance [19-21]. On the other hand, vinyltrimethoxysilane as the most commonly used silane precursor is widely used to enhance both the mechanical and thermal properties of polymer materials [22]. Therefore, in the present study, we adopt DOPO-VTS to coat on the surface of ZHS through a simple method thereby affording a new organic-inorganic hybrids, DOPO-VTS-ZHS nanocomposite. As-obtained DOPO-VTS-ZHS nanocomposite was incorporated into PVC matrix so as to reduce fire hazard and increase flame retardancy. This article deals with the structure characterization of DOPO-VTS-ZHS doped PVC composite and the effect of the synergistic effect between DOPO-VTS and ZHS nanoparticles on the thermal stability, combustion performance and mechanical properties of the PVC-matrix composite.

2. Experimental methods

2. 1 Materials used

$C_2H_4(NH_2)_2$ [1,2-ethanediamine (EN), Tianjin Kermel Chemical Reagent Company, Tianjin, China], C_2H_5OH (ethanol, Anhui Ante Food Company Limited, Anhui, China), $NaSnO_3 \cdot 4H_2O$ (sodium stanante tetrahydrate, Sinopharm Chemical Reagent Company, Shanghai, China), $ZnSO_4 \cdot 7H_2O$ (zinc sulfate heptahydrate, Tianjin Kermel Chemical Reagent Company, Tianjin, China) and epoxy polyester (abridged as EP, Feicheng Deyuan Chemicals Company Limited, Shandong China) were commercially obtained. Deionized water was prepared at in our laboratory. All reagents were used as received without further experimental purification.

2. 2 Preparation of DOPO-VTS and ZHS nanoparticles

DOPO-VTS was prepared by the previously reported method [23]. ZHS was prepared with liquid-phase route. Briefly, 0.27 g of $ZnSO_4 \cdot 7H_2O$ was added to 100 mL of distilled water in a 250-mL flask under magnetic stirring to form a transparent solution. Then 0.28 g of $NaSnO_3 \cdot 4H_2O$ was dissolved in 20 mL of distilled water and was added into the flask. The reaction system was maintained at 5 ^oC for 5 h. Finally, 0.27 g of $ZnSO_4 \cdot 7H_2O$ was added into the reaction system and kept in an ice bath under stirring for additional 1 h. The crude precipitate, a white powder, was collected by filtration. Resultant crude precipitate was washed with distilled water for several times and dried at 80 ^oC in air for 12 h affording ZHS nanoparticles.

2. 3 Preparation of DOPO-VTS-ZHS nanocomposite

The as-prepared ZHS (3.0 g) was dispersed in 60 mL of distilled water and sonicated for 30 min in an ultrasonic bath. Resultant transparent solution was transferred into a 250 mL three-neck-round-bottomed glass flask equipped with a temperature controller, a magnetic stirrer and a reflux condenser. Besides, DOPO-VTS (6 g) was pre-dissolved in 40 mL of ethanol and then added into the flask, followed by the dropwise addition of 2 mL of ammonia. The mixed reaction solution was heated slowly to 80 ^oC and held there for 5 h to allow the functionalization process to finish. Upon completion of the reaction, the reaction mixture was separated by filtration, and the precipitate was thoroughly washed with ethanol and distilled water to afford the target product after drying overnight at 80 ^oC in vacuum.

2. 4 Preparation of DOPO-VTS-ZHS/PVC nanocomposites

The preparation of PVC composite doped with 5.0 wt.% DOPO-VTS-ZHS is illustrated below as an example. DOPO-VTS-ZHS (6.0 g) nanocomposite, stearic acid (0.96 g), lead stearate (0.72 g), calcium stearate (0.72 g) and dioctyl phthalate (DOP; 48 g) were mixed with PVC powder (120 g) on a S(X) K-160 rubber & plastics mixing mill (Shanghai Light Industry Machinery Company Ltd.; Shanghai, China) at 110 °C (milling for 10 min). The mixture was compression molded at 165 °C and 10 MPa for 5 min to afford the plates with a suitable thickness (100 × 100 × 3 mm^3). The samples of

neat PVC, ZHS/PVC and DOPO-VTS/PVC were prepared in the same manner.

2. 5 Apparatus and experimental method

X-ray powder diffraction (XRD) patterns were collected on a X' Pert Pro diffractometer using Cu Kα radiation (λ=0.15418 nm). The operation voltage and current were 40 kV and 40 mA, respectively. Transmission electron microscopy (TEM) images were obtained on a JEM-2010 microscope. The samples were prepared by placing a drop of primary sample on a copper grid, which was covered by carbon film, and the samples were required to dry completely at ambient temperature. Fourier transform infrared (FT-IR) spectrum was measured on an Avatar360 FT-IR spectrometer using KBr pellet. Background correction was made using a reference blank KBr pellet. X-ray photoelectron spectroscope (XPS) analysis was performed on an Axis Ultra multifunctional X-ray photoelectron spectrometer, using Al Kα excitation radiation ($h\nu$ = 1486.6 eV). Thermogravity analysis (TGA) was conducted on a DSC6200 thermal analyzer instrument. About 3.0 mg of the sample was measured from room temperature to 600 ^{o}C at a linear heating rate of 10 ^{o}C /min under air atmosphere (gas flow rate of 150 ml/ min). An HC-2 oxygen index meter (Jiangning Analysis Instrument Company, Nanjing, China) was performed to measure the limiting oxygen index (LOI) values. According to ASTMD2863, the specimens used for LOI were of dimensions 100 × 6.5 × 3 mm^3. The tensile strength of the nanocomposites was measured according to the Chinese standard method (GB T1040-92) with a WDW-10D electronic universal testing instrument (Jinan Test Metal Group Limited Company) at the crosshead speed of 20 mm·min^{-1} at 23 ^{o}C. Cone calorimetry (Fire Testing Technology, U. K.) test was carried out following the procedures in ISO5660. Each specimen with the dimensions of 100×100×3mm^3 was exposed to 35 kW/m^2 heat flux.

3. Results and discussion

3. 1 Structure characterization of as-prepared DOPO-VTS-ZHS nanocomposite

Fig. 1 shows the TEM images of as-prepared ZHS nanoparticle and DOPO-VTS-ZHS nanocomposite. It can be seen that as-prepared ZHS nanoparticles exhibit a diameter of 30~40 nm, and their surfaces seem to be slightly fuzzy (Fig. 1a). After ZHS is coated with DOPO-VTS, resultant DOPO-VTS-ZHS nanocomposite has a diameter of 50~60 nm (Fig. 1b), possibly due to Ostwald ripening. Namely, some small particles tend to dissolve and grow on the surface of more bigger ZHS at high temperature. And then the growth ceases, when DOPO coats on the surface of ZHS, which implies that DOPO-VTS is successfully coated on ZHS surface.

XRD measurements were carried out to determine the composition and crystalline phase of the as-prepared samples. Fig. 2 shows the XRD patterns of ZHS and DOPO-VTS-ZHS nanocomposites. The prominent XRD peaks of ZHS nanoparticles and DOPO-VTS-ZHS nanocomposites can be indexed as cube structure phase of ZHS (JCPDS No. 20-1455). In the meantime, no other phases are detected by XRD, which indicates that the surface coating does not cause changes in the crystal structure of ZHS nanoparticles

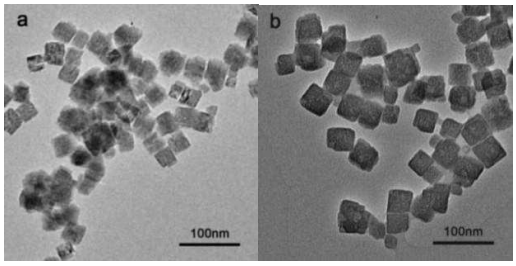

Fig. 1. TEM images of (a)ZHS nanoparticles and (b) DOPO-VTS-ZHS nanocomposites.

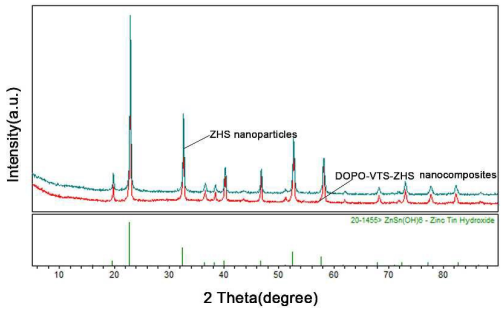

Fig. 2. XRD patterns of ZHS nanoparticles and DOPO-VTS-ZHS nanocomposites.

The chemical structure of ZHS and DOPO-VTS-ZHS was characterized by FT-IR. The FT-IR spectra of ZHS and DOPO-VTS-ZHS are shown in Fig. 3. ZHS shows broad absorption bands around 3238 and 1177 cm^{-1}, and these absorption bands are assigned to O-H vibration. It also shows two peaks around 781 and 539 cm^{-1}, and these absorption peaks are assigned to the characteristic stretching vibration of SnO and ZnO [24]. As a comparison, DOPO-VTS-ZHS shows some new absorption peaks. The peaks at 2929 and 2859 cm^{-1} are attributed to the asymmetric and symmetric C-H stretching vibrations of methyl and methylene groups. The peak at 1270 cm^{-1} represents P=O bending. The absorption bands at 1596 cm^{-1} indicate the existence of P–Ph bonds [25]. Moreover, the peaks at 921 and 1100 cm^{-1} are due to P–O–Ph bonds and Si–O bonds, respectively [26]. All indicate that there is DOPO-VTS in the as-prepared DOPO-VTS-ZHS. Namely, the above mentioned FT-IR spectra confirm that organic-inorganic particles have been successfully coated on the surface of ZHS.

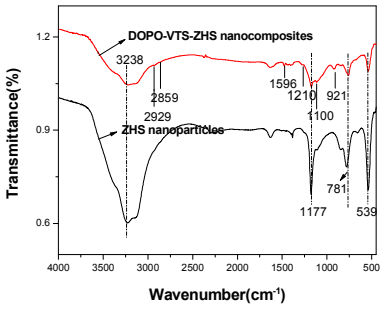

Fig. 3. FT-IR spectra of ZHS nanoparticles and DOPO-VTS – ZHS nanocomposites.

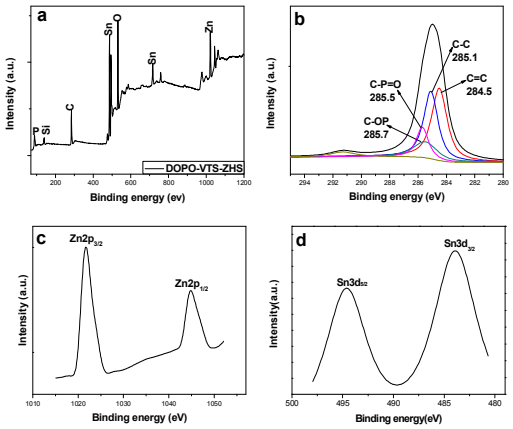

Fig. 4. XPS spectra of the DOPO-VTS-ZHS nanohybrid (a), C1s (b), Zn2p (c) and Sn3d (d).

XPS analysis was further used to reveal the structure of DOPO-VTS-ZHS nanocomposite. In Fig. 4a, it can be seen that the product contains C, O, Si, P, Zn and Sn elements. Particularly, in Fig. 4b, the high resolution C1s peak of the DOPO-VTS-ZHS nanocomposite can be deconvoluted into four components corresponding to carbon atoms in different functional groups: the C=C group (284.5 eV), C-C group (285.1 eV), C-P=O group (285.5 eV) and C-OP group (285.7 eV). Combined with the presence of the peak of silicon element (Fig. 4a), these prove that there are DOPO-VTS in the sample. In addition, two peaks at 1021.8 and 1044.8 eV (Fig. 4c) correspond to Zn2p3/2 and Zn2p1/2, respectively; The peaks at 484.9 and 493.3 eV (Fig. 4d) are corresponded to Sn3d5/2 and Sn3d3/2; These indicate there are Zn and Sn elements, which are belonged to ZHS nanoparticles. Therefore, the XPS results further proved that the DOPO-VTS has successfully coated on the surfaced of ZHS nanoparticles.

3. 2 Wetability and TGA of as-prepared DOPO-VTS-ZHS nanocomposite

Wettability as a very important physico-chemical property of materials is governed by both the surface chemical composition and geometric structure. Fig. 5 shows the profile of the water droplets on ZHS and DOPO-VTS-ZHS. As-prepared ZHS nanoparticles can be easily wetted by water. Namely, water is immediately spread over ZHS upon dripping (Fig. 5a), which indicates that ZHS nanoparticles are of high hydrophilicity. Differing from ZHS nanoparticles, DOPO-VTS-ZHS nanocomposite can hardly be wetted by water and exhibit a large water contact angle of 90.8°, which demonstrates that the coating of ZHS by DOPO-VTS leads to drastically increased hydrophobicity. This also proves that DOPO-VTS is successfully coated on the surface of ZHS.

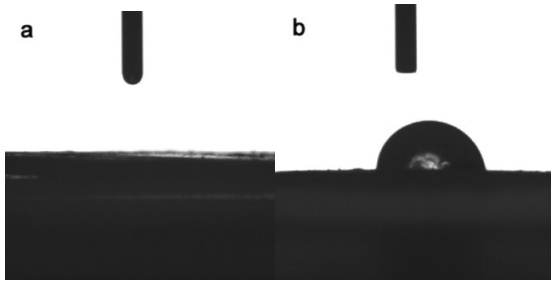

Fig. 5. Profile of the water droplet with a contact angle of (a) ZHS and (b) DOPO-VTS- ZHS.

To estimate the amount of DOPO-VTS on the surface of ZHS, we conducted TG analysis of samples ZHS, DOPO-VTS and DOPO-VTS-ZHS. Fig. 6 illustrates the TG curves of ZHS, DOPO-VTS and DOPO-VTS-ZHS under air atmospheres. For ZHS, the mass loss is the lowest, 21%, which is mainly due to the dehydroxylation of $ZnSn(OH)_6$ generating $ZnSnO_3$. For DOPO-VTS, the mass loss is the highest, 77%, which is mainly attributed to the oxidation of DOPO-VTS producing volatiles of CO, CO_2, H_2O, etc. As for DOPO-VTS-ZHS, the weight loss is 25%, between ZHS and DOPO-VTS, which should be closely related to the dehydroxylation of ZHS and oxidation of DOPO-VTS. The results indicate DOPO-VTS has coated on the surface of ZHS. Furthermore, the content of DOPO-VTS in DOPO-VTS-ZHS nanocomposite can be calculated according to the above TGA results, which is about 7.14 wt.%.

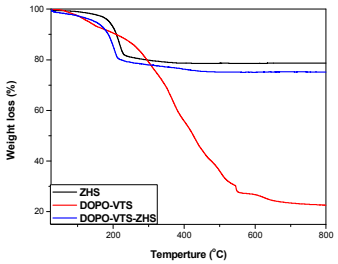

Fig. 6. TGA curves of ZHS nanoparticles and DOPO-VTS-ZHS nanocomposites under air atmospheres.

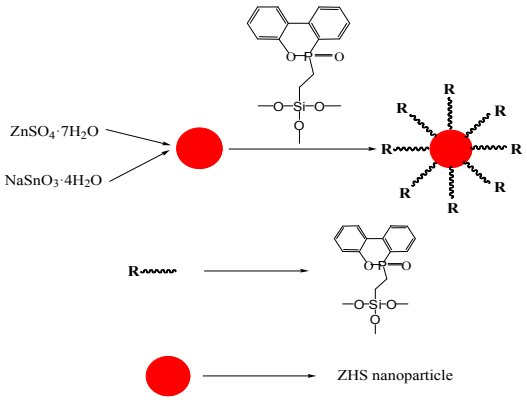

Fig. 7. Schematic diagram showing possible coating process of DOPO-VTS-ZHS nanocomposites.

Fig. 7 shows a schematic diagram to illustrate possible coating process of DOPO-VTS-ZHS nanocomposites. Briefly, the formation and growth of DOPO-VTS-ZHS nanocomposites roughly involve two consecutive steps. The first step involves the nucleation and growth of ZHS nanocore by way of chemical reaction. At the second step, DOPO-VTS molecules are attracted by and anchored onto the surface of during the surface coating process thereby preventing the growth and agglomeration of ZHS nanoparticles and giving rise to desired DOPO-VTS-ZHS nanocomposites.

3. 3 SEM morphology of ZHS/PVC and DOPO-VTS-ZHS/PVC nanocomposites

The properties of the nanocomposites depend strongly on the dispersion state of nanofillers in the polymer matrix. Fig. 8 shows the SEM images of ZHS/PVC and DOPO-VTS-ZHS/PVC nanocomposites. It can be seen that ZHS nanoparticles are unevenly dispersed in PVC matrix, and they tend to aggregate to some extent (Fig. 8a). Contrary to the above, the DOPO-VTS-ZHS nanoparticles are uniformly dispersed in PVC matrix and show few aggregation than ZHS nanoparticles (Fig. 8b), which confirms that DOPO-VTS-ZHS nanoparticles exhibit good dispersibility in the polymeric matrix. This is because the DOPO-VTS species in the DOPO-VTS-ZHS nanoparticles help to improve the compatibility between PVC matrix and ZHS nanoparticles. Namely, the good dispersion of DOPO-VTS-ZHS can be attributed to the strong interfacial interaction between the coated ZHS nanoparticles and the PVC matrix.

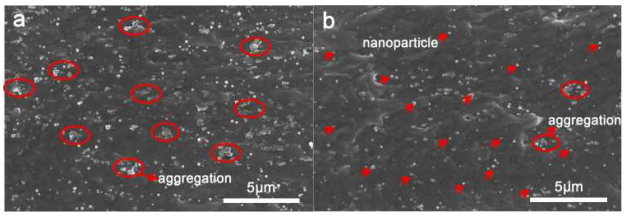

Fig. 8. SEM photographs of (a) ZHS/PVC, (b) DOPO-VTS-ZHS/PVC nanocomposites.

3. 4 Thermal degradation and LOI of PVC and its nanocomposites

The TGA and DTG profiles for PVC and its nanocomposites as a function of temperature in air atmospheres are shown in Fig. 9, and the related data are recorded in Table 1. In comparison with those of

neat PVC, the 5% weight loss (T_{d5}) and maximum degradation ($T_{d,max}$) temperature of the ZHS/PVC nanocomposite were decreased. At the same time, the DTG curves (Fig. 9b) show the maximum mass loss rate (the peak of DTG curves) notably increases. This is because ZHS can react with Cl• to form Lewis acids $SnCl_2$ and $ZnCl_2$ that can catalyze dehydrochlorination and promote early crosslinking of PVC thereby leading to rapid charring [27]. After introducing DOPO-VTS into PVC matrix, the T_{d5}, $T_{d,max}$ and the maximum mass loss rate of DOPO-VTS/PVC nanocomposite were slightly lower than that of pure PVC, possibly because the phosphorous group degraded at relatively low temperatures. This phenomenon played an important role in improving the flame retardancy of the polymer. When ignited, the phosphorous group degraded at first and the decomposition of phosphate group formed a phosphorus-rich residue to prevent further decomposition of the polymer matrix [28]. As for the DOPO-VTS-ZHS/PVC, which presents a similar degradation behavior to that of the ZHS/PVC. This is mainly due to the contribution of ZHS because ZHS holds the highest content in DOPO-VTS-ZHS. As far as the char yield is concerned, the presence of ZHS, DOPO-VTS and DOPO-VTS-ZHS in the PVC matrix lead to increase the char yield at 600 °C. Particularly, the char yield of DOPO-VTS-ZHS/PVC is the highest, suggesting a synergistic effect for char formation between DOPO-VTS and ZHS. The improved char residue provides a protective shield of mass and heat transfer between air and PVC matrix, which can slow down the heat release rate during combustion.

LOI, an important parameter for evaluating the flame retardancy of materials is the minimum oxygen concentration by volume for maintaining the burning of polymers. Therefore, LOI was also measured and the data was shown in Table 1. It can be seen that LOI values of both DOPO-VTS/PVC and ZHS/PVC nanocomposites are higher than that of neat flexible PVC (25.8%). After DOPO-VTS-ZHS nanoparticles are incorporated in PVC matrix, the LOI value significantly rises from 25.8% to 30.2%; and this finding is consistent with corresponding char yield of the composites. Therefore, it can be concluded that, at a low loading, DOPO-VTS-ZHS nanoparticles impart the good flame retardancy of flexible PVC.

3.5 Evaluation of fire hazard by cone calorimetry

Cone calorimetry has been widely used to evaluate the flammability of various materials under real-world fire conditions. Some important parameters are obtained from the cone calorimeter tests, such as peak heat release rate (pHRR), total heat release (THR), total smoke production (TSP) and average mass rate (AMLR) as summarized in Table 2. The HRR and THR of the nanocomposites with different flame retardants are shown in Fig. 10. It is shown that PVC burns extremely rapidly after ignition and the pHRR value reaches 355.4 Kw/m^2. DOPO-VTS is usually used to impart flame retardant properties to polymers because it is responsible for the reduced pHRR. As expected, incorporating DOPO-VTS into PVC decreases pHRR to 340.2 Kw/m^2. For ZHS/PVC, the pHRR decreases to 243.5 Kw/m^2. In addition, the pHRR for DOPO-VTS-ZHS/PVC shows a further reduction compared to that of DOPO-VTS/PVC or ZHS/PVC. Simultaneously, the THR values of PVC composites are significantly lowered after incorporating DOPO-VTS or ZHS. When DOPO-VTS-ZHS is incorporated into the PVC, the flame retardant resins exhibit the lowest THR value. Those indicate that there is a synergistic effect between DOPO-VTS and ZHS. We think that the synergistic effects mainly show in three respects: the DOPO-VTS coated on ZHS nanoparticles prevent the ZHS from agglomeration, resulting in the good dispersion and the enhancement of mechanical property; the ZHS and DOPO-VTS can play their roles in gas phase during the thermal degradation process because they all can capture free radicals to dilute the concentration of combustible gas and oxygen; the ZHS and phosphates can act as corsslinkers or catalytic charring agents in the condensed phase and the silicon also reinforced effects in the condensed phase.

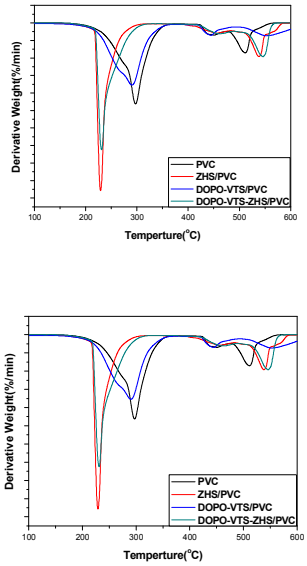

Fig. 9. TGA and DTG curves of pure PVC, ZHS/PVC, DOPO-VTS/PVC, and DOPO-VTS-ZHS/PVC.

Table 1. Summary of the parameters of thermal and mechanical properties.

Sample	T_{d5} (°C)	T_{dmax}(°C)	Char yield	LOI (%)	Tensile strength (MPa)
PVC	237.5	297.5	0.63	25.8±0.1	16.22±0.4
ZHS/PVC	224.2	229.3	0.82	28.9±0.1	16.53±0.2
DOPO-VTS/PVC	220.8	290.6	0.75	26.6±0.1	16.27±0.2
DOPO-VTS-ZHS/PVC	227.4	231.1	1.36	30.2±0.1	18.25±0.3

T_{d5}: the temperature of 5 wt. % weight loss. $T_{d,max}$: the maximum decomposition temperature of the first-derivative profiles.

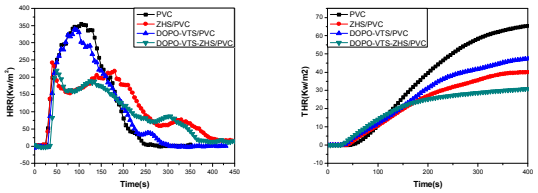

Fig. 10. HRR and THR versus time curves of PVC and its nanocomposites obtained from cone calorimetry test.

3. 6 Smoke suppression properties

The smoke behavior of the materials, which causes most of the casualties during a fire, was investigated by cone calorimetry. The curves of the smoke production rate (SPR) and total smoke release (TSR) of local PVC and its nanocomposites as a function of time are presented in Fig. 11. The TSR values of PVC composites filled with DOPO-VTS, ZHS and DOPO-VTS-ZHS are significantly lower than that of pure PVC; and DOPO-VTS-ZHS nanocomposite exhibits the best smoke suppression towards PVC (the reduction in TSR is up to 59.8%). Meanwhile, the incorporation of DOPO-VTS reduces the SPR value of PVC slightly. After ZHS or DOPO-VTS-ZHS is incorporated into the PVC matrix, the SPR values decrease distinctly. Besides, DOPO-VTS-ZHS/PVC and ZHS/PVC nanocomposites have nearly the same maximum SPR value. However, as compared with ZHS/PVC nanocomposite, the SPR of DOPO-VTS-ZHS/PVC nanocomposite is reduced, especially after 150 s of cone calorimetric test. Above all, the incorporation of DOPO-VTS-ZHS can significantly improve the smoke suppression properties of PVC. Moreover, as listed in Table 2, DOPO-VTS-ZHS/PVC nanocomposite exhibits the lowest AMLR, which conforms well to corresponding TG, SPR and TSR results.

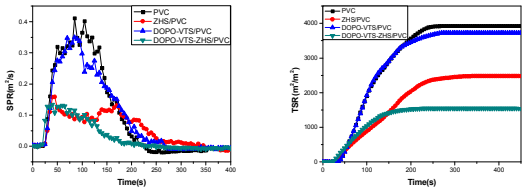

Fig. 11. Smoke production rate and total smoke release curves of PVC and its nanocomposites obtained from the cone calorimetry test.

Table 2. Cone calorimetric data of pure PVC, ZHA/PVC, DOPO-VTS/PVC and DOPO-VTS-ZHS/PVC

sample	pHRR(w · g^{-1})	THR(KJ · g^{-1})	TSR(m^2 · m^{-2})	AMLR(g · s^{-1})
PVC	355.4	65.3	3936.8	0.32
ZHS/PVC	243.5	39.9	2483.8	0.2
DOPO-VTS/PVC	340.2	47.5	3740.3	0.29
DOPO-VTS-ZHS/PVC	216.9	32.7	1580.7	0.18

pHRR: the peak heat release rate; THR: total heat release; TSR: total smoke release; AMLR: average mass loss rate.

3. 7 Char morphology analysis

It is known that the effective protection of the char layer could improve the flame retardancy during combustion. The morphology of the char residues was examined by SEM. Fig. 12 shows the morphology of the outer and inner chars of ZHS/PVC (a and b) and DOPO-VTS-ZHS/PVC (c and d) after LOI test. It is seen that the char of ZHS/PVC nanocomposite is extremely messy and seems to have been crushed, while big air holes appear in the outer char layer. Unlike ZHS/PVC, DOPO-VTS-ZHS/PVC exhibits more smooth and continuous residual char at the outer surface and a more coherent and compact honeycomb-like char in the inner char layer. The honeycomb-like char implies that DOPO-VTS-ZHS/PVC nanocomposite may exhibit much better heat insulation than ZHS/PVC nanocomposite [28], which is due to the synergistic effect between DOPO-VTS and ZHS affording a coherent and compact

char layer to provide improved flame shield for the underlying material during the combustion.

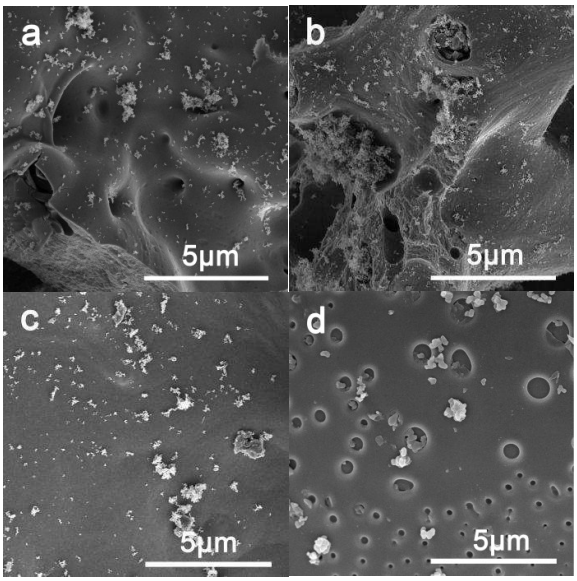

Fig. 12.SEM images of the outer char residue of (a) ZHS/PVC, (c) DOPO-VTS-ZHS/PVC and the inner char residue of (b) ZHS/PVC, (d) DOPO-VTS-ZHS/PVC

3. 8 The mechanical properties of PVC and PVC-matrix nanocomposites

The mechanical properties of PVC and its nanocomposites were evaluated by tensile tests. As shown in Table 1, neat PVC has a high tensile strength of 16.22 MPa, while ZHS/PVC and DOPO-VTS/PVC nanocomposites have slightly increased tensile strength as compared with neat PVC. Differing from ZHS/PVC and DOPO-VTS/PVC nanocomposites, DOPO-VTS-ZHS/PVC exhibits an increased tensile strength of 18.25 MPa, due to the strong interfacial interaction between ZHS and DOPO-VTS. This means that DOPO-VTS-ZHS as a flame retardant of PVC is advantageous over ZHS in terms of well retained mechanical properties of the polymer matrix.

4. Conclusions

DOPO-VTS-ZHS nanocomposites were successfully synthesized by a solution reaction method, and their structure was verified by FT-IR, XRD, TEM and TGA. As-obtained DOPO-VTS-ZHS nanocomposites were doped into PVC matrix to afford DOPO-VTS-ZHS/PVC nanocomposite, and the thermal properties and flame retradancy of the as-fabricated PVC-matrix nanocomposites were investigated. Findings indicate that the incorporation of DOPO-VTS-ZHS leads to significant improvement in the formation of the char residual of PVC in air compared with ZHS, DOPO-VTS. Moreover, as compared with neat PVC, DOPO-VTS-ZHS/PVC nanocomposite undergoes suppressed combustion, which means DOPO-VTS-ZHS is highly effective in reducing the fire hazard of PVC. Furthermore, DOPO-VTS-ZHS/PVC nanocomposite has much higher limiting oxygen index and better mechanical properties than neat PVC. In summary, the improved flame retardancy of DOPO-VTS-ZHS/PVC nanocomposite is attributed to the synergistic flame retardant effect between ZHS nanoparticles and DOPO-VTS, while they both promote catalytic char to lead to form a more coherent and compact honeycomb-like char that can inhibit the release of heat within the char.

Acknowledgments

The authors acknowledge the financial support provided by National Basic Research Program of China, Grant No. 2015CB654700 (2015CB674703) and National Natural Science Foundation of China, Grant No. 21371050.

Notes and references

1 R. Chai, S. Chen and J. Zhang, *J. Appl. Polym. Sci.*, 2012, **125**, 3376-3384.

2 Y. T. Pan and D. Y. Wang, *RSC Adv.*, 2015, **5**, 27837–27843.

3 P. Jia, M. Zhang, C. Liu, L. Hu, G. Feng, C. Bo and Y. Zhou, *RSC Adv.*, 2015,**5**, 41169-41178.

4 A. W. Coaker, *J. Vinyl Addit. Technol.*, 2003, **9**, 108–115.

5 L. Yu, L. Chen, L. P. Dong, L. J. Li and Y. Z. Wang, *RSC Adv.*, 2014, **4**, 17812-17821.

6 T. Kashiwagi, F. M. Du, J. F. Douglas, K. I. Winey, R. H. Harris and J. R. Shields, *Nat. Mater.*, 2005, **4**, 928-933.

7 X. Qian, L. Song, B. Wang, Y. Hu and R. K. K. Yuen, *Mater. Chem. Phys.*, 2013, **139**, 443-449.

8 G. Wrobel, M. Piech, S. Dardona, Y. Ding and P. X. Gao, *Cryst. Growth Des.*, 2009, **9**, 4456-4460.

9 P. A. Cusack, M. S. Heer and A. W. Monk, *Polym. Degrad. Stab.*, 1997, **58**, 229-237.

10 P. A. Cusack, M. S. Heer and A.W. Monk, *Polym. Degrad. Stab.*, 1991, **32**, 177-190.

11 F. Andre, P. A. Cusack, A. W. Monk and R. Seangprasertkij, *Polym. Degrad. Stab.*, 1993, **40**, 267-273.

12 Z. Qin, Y. H. Huang, Q. Y. Wang, J. J. Qi, X. J. Xing and Y. Zhang, *CrystEngComm.*, 2010, **12**, 4156-4160.

13 N. Wu, C. Ding and R. Yang, *Polym. Degrad. Stab.*, 2010, **95**, 2589-2595.

14 X. Su, Y. Yi, J. Tao and H. Qi, *Polym. Degrad. Stab.*, 2012, **97**, 2128-2135.

15 S. H. Liao, P. L. Liu, M. C. Hsiao, C. C. Teng, C. A. Wang, M.-D. Ger and C. L. Chiang, *Ind. Eng. Chem. Res.*, 2012, **51**, 4573-4581.

16 Y. Ni, S. Zheng and K. Nie, *Polymer*, 2004, **45**, 5557-5568.

17 W. Tang, M. H. Santare and S. G. Advani, *Carbon*, 2003, **41**, 2779-2785.

18 X. Qian, L. Song, B. Yu, B. Wang, B. Yuan, Y. Shi, Y. Hu and R. K. K. Yuen, *J. Mater. Chem. A*, 2013, **1**, 6822-6830.

19 B. Perret, B. Schartel, K. Stös, M. Ciesielski, J. Diederichs, M. Döring, J. Krä mer and V. Altstä dt, *Eur. Polym. J.*, 2011, **47**, 1081-1089.

20 A. Schäfer, S. Seibold, O. Walter and M. Döring, *Polym. Degrad. Stab.*, 2008, **93**, 557-560.

21 X. Qian, H. Pan, W. Y. Xing, L. Song, R. K. K. Yuen and Y. Hu, *Ind. Eng. Chem. Res.*, 2012, **51**, 85-94.

22 Y. Xia and R. C. Larock, *Macromol. Rapid. Commun.*, 2011, **32**, 1331-1337.

23 Y. L. Liu, *Polymer*, 2001, **42**, 3445-3454.

24 P. R. Hornsby, P. A. Cusack, M. Cross, A. T´oth, B. Zelei and G. Marosi, *J. Mater. Sci.*, 2003, **38**, 2893-2899.

25 X. Qian, L. Song, B. Yu, B. Wang, B. Yuan, Y. Shi, Y. Hu and R. K. K. Yuen, *J. Mater. Chem. A*, 2013, **1**, 6822-6830.

26 V. C. Tung, M. J. Allen, Y. Yang and R. B. Kaner, *Nat. Nanotechnol.*, 2009, **4**, 25-29.

27 X. Su, Y. Yi, J. Tao and H. Qi, *Polym. Degrad. Stab.*, 2012, **97**, 2128-2135.

28 X. Qian, B. Yu, C. Bao, L. Song, B. Wang, W. Xing, Y. Hu and R. K. K. Yuen, *J. Mater. Chem. A*, 2013, **1**, 9827-9836.